molecules

MDPI

Article

Synthesis, Structural Characterization and Antimicrobial Activity of Cu(II) and Fe(III) Complexes Incorporating Azo-Azomethine Ligand

Mohammad Azam [1,*], Saud I. Al-Resayes [1], Saikh Mohammad Wabaidur [1], Mohammad Altaf [1], Bhaskar Chaurasia [2], Mahboob Alam [3], Satyendra Nath Shukla [2], Pratiksha Gaur [2], Nader Talmas M. Albaqami [1], Mohammad Shahidul Islam [1] and Soonheum Park [4]

1 Department of Chemistry, College of Science, King Saud University, P.O. Box 2455, Riyadh 11451, Saudi Arabia; sresayes@ksu.edu.sa (S.I.A.-R.); tarabai22@gmail.com (S.M.W.); altafamu@gmail.com (M.A.); nader___t@hotmail.com (N.T.M.A.); shahid10amui@gmail.com (M.S.I.)
2 Coordination Chemistry Research Laboratory, Department of Chemistry, Govt. Science College, Jabalpur 482001, India; bc3088@gmail.com (B.C.); ccrl_2004@rediffmail.com (S.N.S.); drgaur26@gmail.com (P.G.)
3 Division of Chemistry and Biotechnology, Dongguk University, 123 Dongdae-ro, Gyeongju 780-714, Korea; mahboobchem@gmail.com
4 Department of Advanced Materials Chemistry, Dongguk University, 123 Dongdae-ro, Gyeongju 780-714, Korea; shpark@dongguk.ac.kr
* Correspondence: azam_res@yahoo.com; Tel./Fax: +966-11-467-5982

Received: 6 March 2018; Accepted: 27 March 2018; Published: 2 April 2018

Abstract: We are reporting a novel azo-azomethine ligand, HL and its complexes with Cu(II) and Fe(III) ions. The ligand and its complexes are characterized by various physico-chemical techniques using C,H,N analyses, FT-IR, ^{1}H-NMR, ESI-MS and UV-Vis studies. TGA analyses reveal complexes are sufficiently stable and undergo two-step degradation processes. The redox behavior of the complexes was evaluated by cyclic voltammetry. Furthermore, the ligand and its complexes were tested for antimicrobial activity against bacterial and fungal strains by determining inhibition zone, minimal inhibitory concentration (MIC) and minimal bactericidal concentration (MBC). The complexes showed moderate antimicrobial activity when tested against Gram +ve and Gram −ve bacterial strains. To obtain insights into the structure of ligand, DFT studies are recorded. The results obtained are quite close to the experimental results. In addition, the energy gap, chemical hardness, softness, electronegativity, electrophilic index and chemical potential were calculated using HOMO, LUMO energy value of ligand.

Keywords: azo ligand; synthesis; DFT studies

1. Introduction

Over the years, the azo compounds with at least one azo (–N=N–) group, separated by two phenyl rings, have received tremendous attention both in fundamental and applied research [1–6]. Furthermore, the azo compounds are used extensively in textile industry, printing systems, biological staining and various photochemical productions [7–9]. In addition, the azo-Schiff bases are reported to display various antimicrobial, anticancer and antioxidant activities, and several other pharmacological properties [3,10–14].

Over the last few decades, several antibacterial and antifungal drugs, such aspenicillin, cephalosporins, tetracyclines, macrolides and oxaolidinones, fluconazole, ketoconazole and miconazole are being explored to treat the infection caused by various microorganisms [15]. However, there are

reports stating that bacteria release specific things out of the cell, thus making the access of antibiotic to the active site limited, and prevents the accumulation of antibiotic in the interior of the cell, and thus inhibit the action of antimicrobial drug [16]. For example, the β-lactam antibiotic inhibits penicillin-binding proteins (PBPs), an enzyme required for the biosynthesis of bacterial cell wall, is now suffering from resistance due to the release of β-lactamases enzyme, making the drug inactive [17,18]. Similarly, significant occurrence of methicillin-resistant *S. aureus* (MRSA) is steadily rising [19–21]. In last two decades, several new antibiotics failed to meet the challenges posed by multidrug-resistant pathogens [19–21]. Therefore, we need such drugs which are sufficient to counteract and control the antibiotic resistance [19–21]. Over the years, various metal containing compounds have received significant attention in various biological applications, especially anticancer and antimalarial therapy. However, less attention has been given to develop the metal containing antibacterial drugs [20,22]. Therefore, investigations for metal-based antibacterial compounds are required as it anticipated that metal-based drugs may be helpful to overcome the development of antibiotic resistance [20].

Herein this article, we are concerned with the synthesis of a novel azo-azomethine ligand, 2-((E)-(pyridin-2-ylimino)methyl)-4-((E)-p-tolyldiazenyl)phenol and its complexes with Cu(II) ion and Fe(III) ions. The structure of ligand and its complexes have been confirmed by elemental analyses, FTIR, NMR ESI-MS, UV/Vis, thermal and electrochemical studies. In addition, DFT studies have been carried to look insights the bonding of the ligand. Furthermore, the ligand and its complexes showed potential antimicrobial activity when screened against Gram +ve and Gram −ve pathogens.

2. Results and Discussion

The synthesis of ligand, HL and its complexes is described in Scheme 1. The mass spectral studies of the azo-Schiff base ligand, HL and its complexes 1 and 2 were recorded by the electron impact mass spectrum and its data are given in experimental section. The molecular ion peak $[M + H]^+$ *m/z* at 316.1, 731.2 and 723.5 are corresponding to their molecular formulae, $C_{19}H_{16}N_4O$, $C_{38}H_{34}CuN_8O_4$and $C_{38}H_{34}FeN_8O_4$, respectively. On the other hand, the calculated *m*/*z* for ligand, HL and its complexes 1 and 2 were found to be 316.4, 730.2 and 722.2, respectively (Supplementary Materials Figure S1). The stoichiometric analyses of ligand, HL and its complexes agree well with their proposed composition.

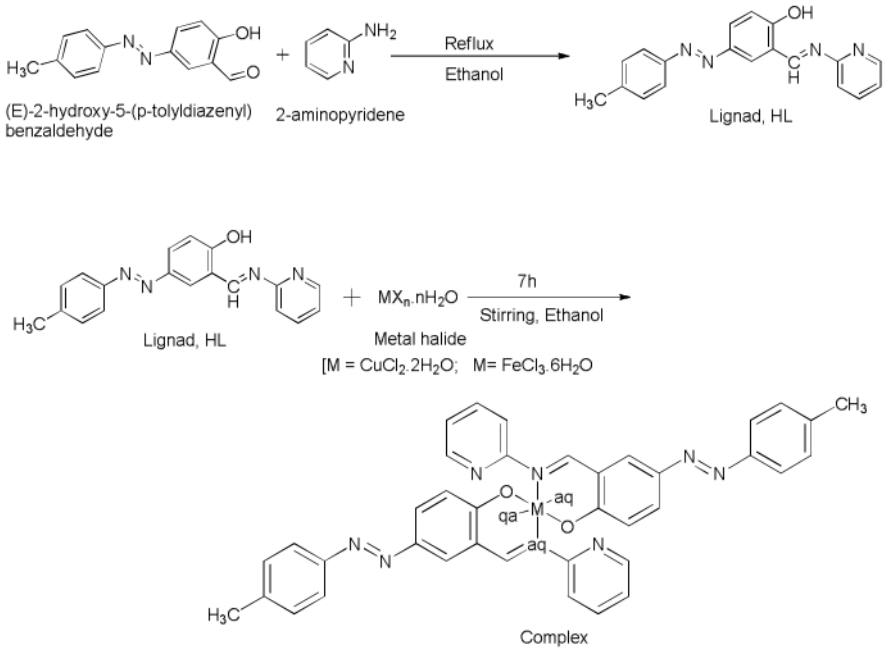

Scheme 1. Preparation of azo-azomethine ligand, HL and its complexes with Cu(II) and Fe(III) ions.

IR spectra of ligand, HL exhibited prominent peaks at 3053 cm^{-1}, 1666 cm^{-1}, 1460 cm^{-1} ascribed to $\nu_{(–OH),}$ $\nu_{(–CH=N)}$ and $\nu_{(N=N)}$ vibrations, respectively [23–26]. In addition, the stretching vibration due to $\nu_{(C–O)}$ band appeared at 1284 cm^{-1} in the free azo-Schiff base ligand [23,24]. However, position of these vibrations shifted from their original values upon complexation to metal ions [3,25–27]. In addition, the strong confirmation for the coordination of metal ion to ligand came from the absence phenolic OH group in the complexes 1 and 2 complexes showing that the coordination took place via the deprotonated OH group of the free azo-Schiff base ligand [3]. However, there was no change noticed in the position of –N=N– (azo group) in the complexes indicating that it did not take part in complex formation [23]. The IR values obtained from the simulated spectrum practically coincide with the experimental results, and are supported by the data reported in literature (Figure 1) [28].

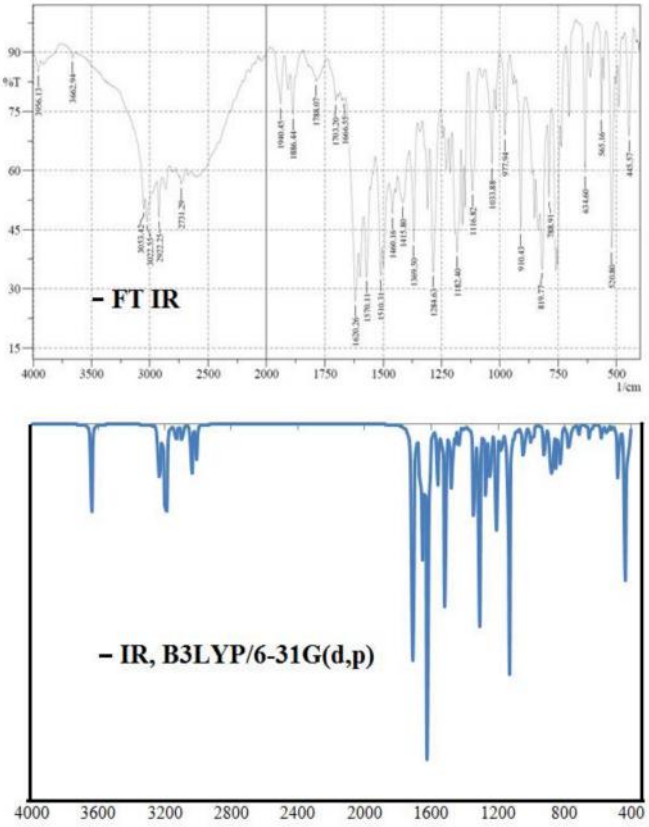

Figure 1. Comparison of experimental and simulated IR spectra of ligand, HL.

The electronic spectrum of ligand (Figure 2) showed absorption bands at λ_{max}250 nm and λ_{max}320 nm due to low energy π-π* transitions [24,29].

To compare the experimental results, theoretical calculation were carried out in the solution as well as in the gaseous state by employing TD-DFT/B3LYP/6-31G(d,p) level of theory for the optimized structure (Figure 2). The observed absorption bands at 320 nm and 250 nm of the ligand in solution are assigned to various HOMO → LUMO transitions. However, the theoretical absorption bands are observed at 380 nm and 345 nm in solution and 402 and 380 nm in vacuum, suggesting that absorption spectrum in solution is closest to the experimental results. These values indicate that the UV in solution is more suitable than the gas phase for studying the absorption spectra of the ligand. The absorption bands are slightly changed to the higher wavelength due to solvent effect.

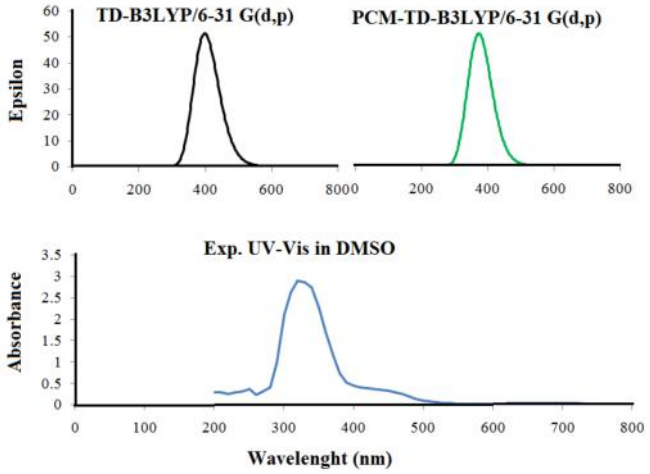

Figure 2. Comparative experimental and theoretical UV/Vis spectra.

However, upon complexation, the position of absorption bands is shifted [30]. Furthermore, broad-band at λ_{max}390 nm is assigned to n-π* transitions of –N=N– chromophore groups [24]. However, there was no significant change in these absorption bands in the complexes. The complex 1 exhibited a broad absorption band at 615 nm assigned to $^2B_{1g} \rightarrow {}^2B_{2g}$ transition indicating an octahedral geometry around Cu(II) ion [31,32], which is further confirmed by the magnetic susceptibility data at 1.7 BM [30]. The complex 2 showed absorption bands at340 nm and 370 nm corresponding to L → M charge transitions [33]. In addition, absorption bands at 440 nm and 510 nm were also observed, and assigned to $^6A_1g \rightarrow {}^4T_{1g}$ and $^6A_{1g} \rightarrow {}^4T_{2g}$and $^2T_2 \rightarrow {}^2A_2$ transition. Moreover, the magnetic moment value at 5.90 B.M suggests an octahedral environment around Fe (III) ion [32] (Supplementary Information Figure S2).

2.1. Frontier Molecular Orbitals—HOMO and LUMO of Ligand

The study of molecular orbitals can bring useful information on the electronic framework and is widely applied in the analysis of chemical reactions [34]. Frontier molecular orbital (FMOs) energies were determined using the B3LYP/6-31G (d,p) level for the optimized molecular structure. The graphical presentation of HOMO, LUMO orbitals and Energy gap (Eg) are shown in Figure 3. The HOMO is largely located on diazo group around azomethine moiety and pyridine N, whereas LUMO is strictly confined over toluidine and phenolic ring. The HOMO-LUMO gap defines the chemical stability, reactivity and electron conductivity. The HOMO-LUMO gap for the ligand is 3.54 eV, suggesting its high reactivity towards bonding with metals. Furthermore, the HOMO energy shows that molecule is susceptible towards the electrophiles, whereas the LUMO energy indicates the susceptibility of the molecule towards the nucleophiles [35]. The chemical reactivity based on various quantum chemical parameters is given in Table 1.

Table 1. Quantum chemical parameters.

	Ligand
HOMO	−0.2040 (−5.50 eV)
LUMO	−0.0722 (−1.96 eV)
ΔE	0.1302 (3.54 eV)
Mulliken Electronegativity χ	0.1373
Global Hardness η	0.0651
Absolute softness σ	15.3609
Chemical Potential μ	−0.1373
Global Softness S	7.6804
Global Electrophilicity ω	0.1447
Electronic Charge ΔN	2.1090
Dipole Moment	3.4276

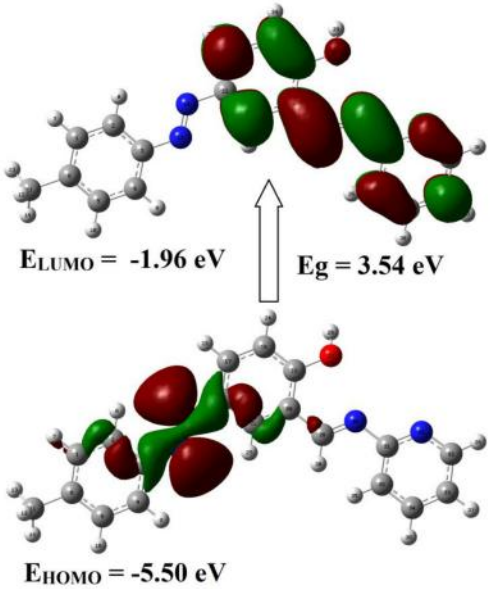

Figure 3. HOMO, LUMO and energy difference of ligand.

2.2. Mulliken Charge Analysis of Ligand

The net atomic charges of the ligand have been described using Mulliken population analysis using B3LYP/6-31G basis set, and have a significant influence on vibrational spectra, dipole moment, molecular polarizability, electron structure and many properties of the molecular skeleton (Figure 4). In the ligand, the more positive charge on C31 + 0.348 carbon atom was due to the fact that this C31 carbon was flanked between two highly electro negative nitrogen, which was caused by the −I effect of nitrogen of azomethine N and Pyridine N atoms. Similarly C19 and H29 have positive charge of +0.324 and +0.329 respectively, due to their attachment with a strongly electronegative O atom. Highly shielded atoms such oxygen and nitrogen attached to less electronegative acquired highly negative charge, phenolic O27 and azomethine N26 being highly shielded having negative charge −0.376 and −0.463 respectively and pyridine N has a charge of −0.397 on the molecular system of the ligand.

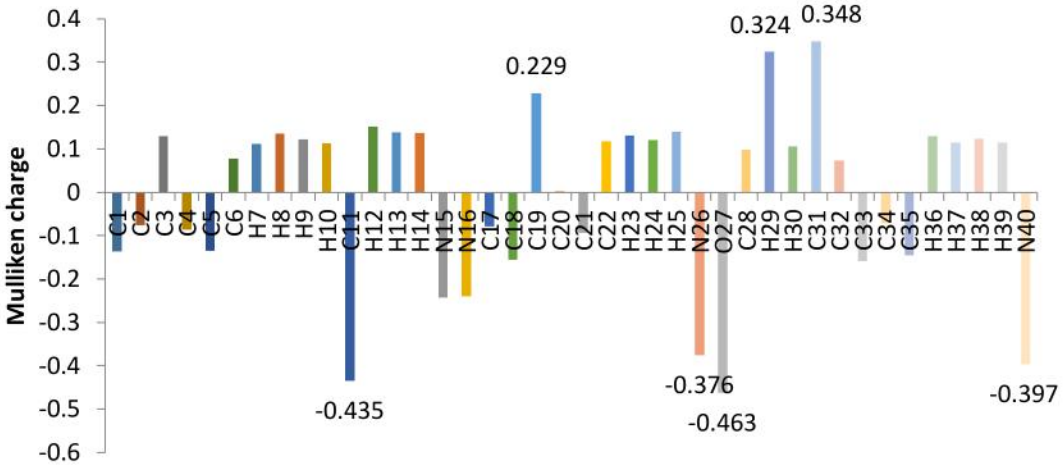

Figure 4. Mulliken Charge Distribution of ligand, HL.

2.3. Molecular Geometry of Ligand

The optimized ligand structure is non-planar and as shown in Figure 5 with the numbering scheme of the atoms. The optimized structural parameters given in Table 2 are comparable to XRD data with the similar structure [29]. It is reported that the optimized structural parameters are slightly different from the experimental results. However, 7° bond angle deviation has been reported for N15-N16-C3 in theoretical and experimental results [36]. Such deviations are likely due to inter/intra-interaction in crystal, whereas the theoretical studies are calculated for single isolated molecule without crystallographic information file (CIF) in vacuum. The minimum energy of the self-consistent field (SCF) of the molecule is −644,785.8000 kcal/mol in vacuum and −644,803.2394 kcal/mol in the solvent confirming that the geometry of the molecule is more stable in solvent phase because of the presence of hydrogen bonds. In addition, the optimized ligand geometry was also validated by frequency calculations, and provided real values for the frequencies obtained, and no imaginary frequency was found. Positive values indicate that the structure has minimal potential energy. Therefore, we can propose an optimized structure (Figure 5) for the ligand on the basis of elemental analyses, FT-IR, Electronic spectra, ^{1}H-NMR, and DFT study.

Table 2. Selected Optimized geometrical parameters of ligand in the ground state.

Bond Length (Å)	B3LYP/6-31G (d,p)	Ref. [6]	Bond Angles (°)	B3LYP/6-31G (d,p)	Literature
N15-N16	1.232	1.25	N15-N16-C22	119.9	112.2
C19-O27	1.430	1.367	N15-N16-C3	120.0	113.4
C28-N26	1.293	1.304	C19-N20-C21	119.9	120.0
C31-N40	1.343	1.341	C19-N20-C28	120.0	121.2
C31-N26	1.399	1.397	Dihedral angles (°)	B3LYP/6-31G (d,p)	Ref
C3-N15	1.470	1.428	C3-N15-N16-C22	−179.9	−178.1
O27-H29	0.960	0.840	C20-C28-N26-C31	−179.9	–
C20-C21	1.401	1.390	C3-N15-N16-C22	−179.9	–
Bond angles (°)	B3LYP/6-31G (d,p)	Ref. [6]	C21-C20-C19-O27	−179.9	−178.4
C28-N26-C31	119.9	116.6	C28-C20-C19-O27	0.0	−1.1
C31-N40-C32	121.4	118.1	C21-C20-C19-C18	0.0	0.0
C19-O27-H29	109.4	109.5	C28-C20-C19-C18	−179.9	178.4

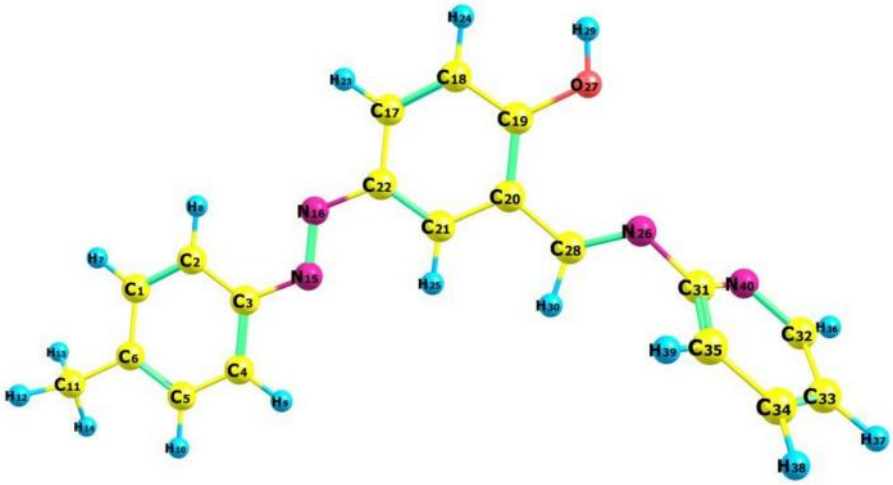

Figure 5. Optimized geometry of the ligand visualized using Chemcraft program.

^{1}H-NMR spectrum of ligand, HL (Figure 6) displayed a set of signals in the range of δ 0–14 ppm corresponding to various positions within the ligand. The singlet due to methyl protons appear at δ 2.20 ppm. The signal is appeared as two doublets at δ 6.93 and δ 7.03 ppm were assigned for toluidine aromatic protons. Similarly the singlet at δ 7.21 for 1H and two doublets at δ 7.20 and δ 7.18 for 1H each, were attributed for all the three protons of phenolic ring. The signal appeared at δ 7.34, δ 7.37

and δ 7.38 ppm were assigned for protons of pyridine ring. A signal at δ 8.62 ppm for 1H was assigned for one azomethine (–CH=N–) proton. Phenolic OH generally resonates at very high frequency in the *deshielding region* of the NMR spectrum. In our study, the ligand shows the phenolic proton as a singlet at δ 13.39 ppm (s, 1H, OH). The ^{1}H-NMR spectrum of ligand has been compared with the experimental data and is given in Figure 6a–d. The calculation of ^{1}H-NMR spectrum was carried out in dimethyl sulfoxide (DMSO) solution using PCM model within GIAO-B3LYP framework. However, the expected NMR chemical shifts were not fully compatible with the experiment results. As can be seen in Figure 6c, some of the peaks such as hydroxyl and methyl protons appeared in spectrum were deviated from standard values, which can be explained on the basis of steric hindrance, solvent effect, and stereochemistry. Furthermore, the effects of the solvent were found for the OH proton to a varying extent. The correlation coefficients of ^{1}H-NMR for ligand were determined to be 0.974 as shown in Figure 6c. (Ligand^{1}Hδ_{cal} = 1.239δ_{exp} − 0.297 (R^2 = 0.974)). Predicted chemical shift values applying linear regression were found to be in reasonable agreement with the experimental values.

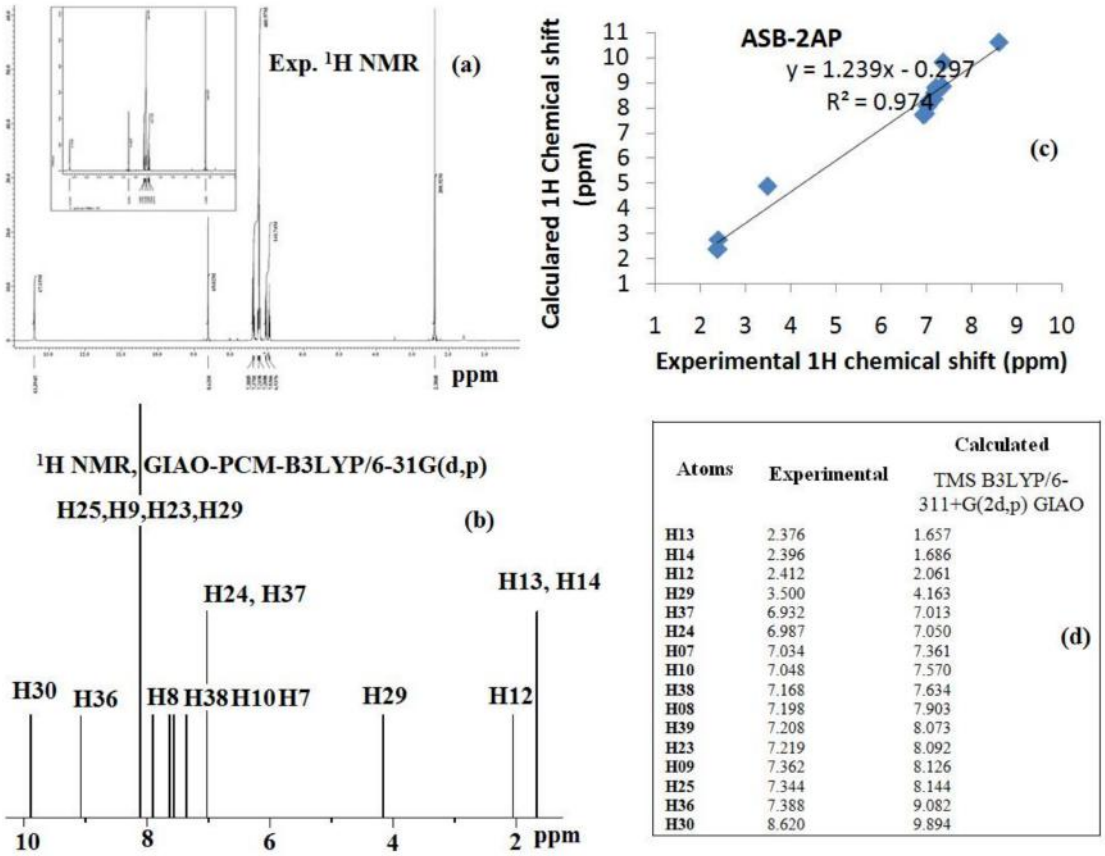

Atoms	Experimental	Calculated TMS B3LYP/6-311+G(2d,p) GIAO
H13	2.376	1.657
H14	2.396	1.686
H12	2.412	2.061
H29	3.500	4.163
H37	6.932	7.013
H24	6.987	7.050
H07	7.034	7.361
H10	7.048	7.570
H38	7.168	7.634
H08	7.198	7.903
H39	7.208	8.073
H23	7.219	8.092
H09	7.362	8.126
H25	7.344	8.144
H36	7.388	9.082
H30	8.620	9.894

(d)

Figure 6. Comparison of (**a**) experimental and (**b**) theoretical ^{1}H-NMR spectra (**c**) correlation graph and (**d**) experimental and calculated ^{1}H chemical shifts (ppm) of ligand, HL.

2.4. Thermal Studies

TGA results (Figure 7) show that both the complexes degrade almost in same way, and the whole degradation occurs in two steps. The first step in both complexes include the loss of both the coordinated water molecules at temperature 160–170 °C, which is attributed to 5.0% of the total weight loss in the complexes 1 and 2. Upon increasing temperature, complexes started degrading and complex 1 finally decomposed at temperature 600–630 °C, corresponding to weight loss (84.11%) leaving copper oxide in the end as end product. However, complex 2 is decomposed completely at temperature 650 °C, which is due to the loss of whole organic moiety (72.9% of the complex), leaving metal oxide in the end as end product.

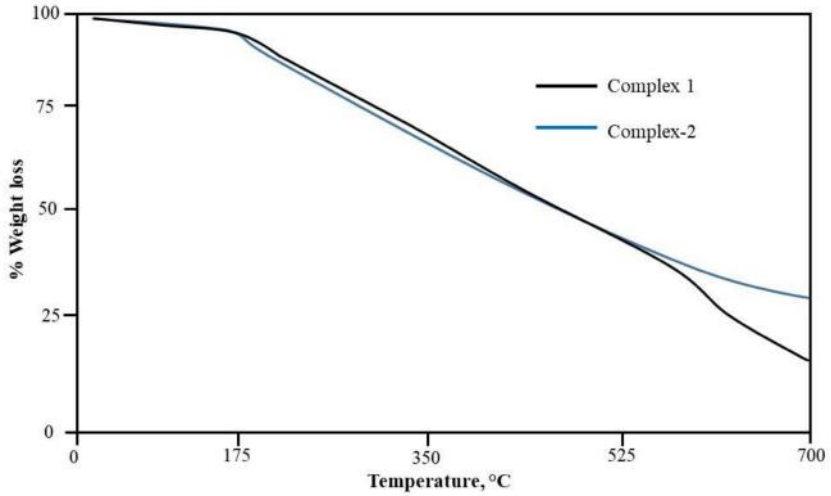

Figure 7. TGA curve of complexes 1 and 2.

The redox properties of complexes 1 and 2 (1.0×10^{-3} mol L^{-1}) were investigated by cyclic voltammetry in the potential range +1.0 to −1.5 V in degassed DMSO solution in the presence tetrabutylammonium perchlorate (0.01 mol L^{-1}) as the supporting electrolyte at a scan rate of 100 mVs^{-1}. The cyclic voltammogram of complex 1 shows two cathodic peaks, observed at potential −1.39 V and −0.92 V and one anodic peak at 0.45 V. However, irreversible oxidation peak is found 0.65 V [37,38]. Complex 2 exhibited two reduction waves at 0.87 V and 0.58 V attributed to the reduction of Fe(III) to Fe(II) and reduction of azo ligand [39,40].

2.5. Antimicrobial Activity

The studied azo-azomethine ligand and its complexes 1 and 2 exhibited significant antimicrobial activity against bacterial strains. However, on comparing the results with the existing antibiotic and antifungal drugs, the ligand and its complexes showed moderate activity against these pathogens. However, ligand and complexes 1 and 2 showed insignificant effect over fungal strains. Interestingly, complexes 1 and 2 exhibited better activity as compared to the free ligand. The complex 1 showed high sensitivity against *E. coli* in comparison to *Streptococcus aureus* (MRSA) (Table 3). The MIC and MBC values obtained for ligand and its complexes against the bacterial and fungal strains are summarized in Table 3. The biological study data in the case of the antibacterial assay discloses that the complexes indicate antimicrobial activity higher than that of the ligand. Such improved activity can be explained on the basis of the theory of chelation.

Table 3. Antimicrobial activity of azo-azomethine ligand and its complexes.

Compound Bacterial Strains	Inhibition Zone (mm)					MIC and MBC (µg/mL)			
	Ligand HL	Complex 1	Complex 2	Cam *	DMSO	MIC (MBC) of HL	MIC (MBC) of complex 1	MIC (MBC) of complex 2	MIC (MBC) of Cam
S. Aureus (MRSA +ve)	7	13	11	17	No zone	512 (512)	128 (128)	256 (256)	32 (32)
E. Coli (Gram −ve)	9	15	17	20	No zone	256 (>256)	64 (256)	256 (>256)	32 (128)
Fungal strains	Ligand HL	Complex 1	Complex 2	Nys *		MIC (MBC) of HL	MIC (MBC) of complex 1	MIC (MBC) of complex 2	MIC (MFC) of Nys
C. Albicans	No zone	No zone	No zone	22	No zone	ND	ND	ND	50 (50)
A. Niger	No zone	No zone	No zone	20	No zone	ND	ND	ND	200 (200)

* Chloramphenicol (Cam) and * Nystatin (Nys) were used as strand drugs for bacteria and fungi, respectively. DMSO was used as a negative control and no effect was detected. ND = Not determined.

3. Materials and Methods

Salicylaldehyde, 2-aminopyridine, $CuCl_2.2H_2O$, $FeCl_3.6H_2O$ were obtained from E. Merck. (E)-2-hydroxy-5-(p-tolyldiazenyl)benzaldehyde used in the synthesis of azo-Schiff base ligand was obtained as reported in literature [2,37]. Electronic absorption spectra were measured using EI-2305 spectrometer. FT-IR spectra were recorded on Shimadzu-8400 PC FT-IR spectrophotometer. ^{1}H-NMR spectra was carried out on Jeol spectrometer at 400 MHz with chemical shifts relative to TMS in d_6-DMSO. The ESI-MS spectra were recorded on an Agilent 6520 (QTOF) mass spectrophotometer. The electrochemical behavior of the complexes was recorded on Ivium technologies potentiostat/galvanostat in a three-electrode cell with glassy carbon (GC) working electrode, a platinum wire auxiliary counter electrode, and Ag/AgCl as a reference electrode. Thermal stability was monitored on SDTQ-600 (TA Instrument) in helium (100 mL min^{-1}) at 20 °C/min at 0–700 °C.

3.1. Synthesis of Ligand, (4E)-4-(2-p-tolyldiazenyl)-2-((E)-(pyridin-2-ylimino)methyl)phenol, HL

An ethanolic solution of (E)-2-hydroxy-5-(p-tolyldiazenyl)benzaldehyde (2.440 g, 10 mmol) was added gradually to the solution of 2-amino pyridine (0.941 g, 10 mmol) dissolved in minimum quantity of same solvent. The resulting reaction mixture was refluxed for 5 h, and allowed to cool at room temperature. A brown colored solid product was obtained, which was removed by filtration and washed with diethylether and dried in vacuum to obtain analytically pure compound.

Color: Brown, yield 68%, mp > 280 °C, molecular formula $C_{19}H_{16}N_4O$; elemental analysis found: C, 72.02; H, 5.02; N, 17.65; Cal. C, 72.13; H, 5.10; N, 17.71%, FT-IR data (KBr, cm^{-1}): 3053 $\nu_{(–OH)}$; 1666 $\nu_{(–CH=N)}$, 1460 $\nu_{(–N=N–)}$; ^{1}H-NMR (DMSO-d_6, 400 MHz, δ in ppm): 8.94 (s, 1H, –CH=N), 2.20 (s, 3H, $–CH_3$), 13.39 (s, 1H, Ar-OH), 6.93–7.38 (m, 11H, Ar-H); electronic spectrum λ_{max}(nm): 250, 320; ESI-mass spectra *m*/*z*: $[C_{19}H_{16}N_4O+H]^+$ 316.1.

3.2. Synthesis of Complexes

3.2.1. Synthesis of Complex 1, $[Cu(L_2)(H_2O)_2]$

$CuCl_2.2H_2O$ (50 mg, 0.292 mmol) was added to the ethanolic solution of azo-Schiff base ligand, HL (185 mg) at room temperature. The resulting reaction mixture was stirred vigorously for 7 h. There was no change noticed in the color of reaction mixture and remains brown. The solution of reaction mixture was reduced under vacuum and precipitated out by adding diethyether, and recrystallized in ethanol. After few days, some brown colored microcsaline product was obtained. Unfortunately, we did not find any crystal suitable for single crystal XRD.

$[Cu(L_2)(H_2O)_2]$: Yield 63.24%, Color: brown, molecular formula $C_{39}H_{37}CuN_8O_4$, elemental analysis found: C, 62.79; H, 4.91; N, 14.91; Cu, 9.02; Cal: C, 62.85; H, 5.00; N, 15.03; FT-IR data (KBr, cm^{-1}): 1673 $\nu_{(–CH=N)}$, 1460 $\nu_{(–N=N–)}$; UV/Vis (λ_{max}nm): 615; ESI-Mass spectra, *m*/*z*: $[C_{38}H_{34}CuN_8O_4 + H]^+ = 731$.

3.2.2. Synthesis of Complex 2, $[Fe(L)_2 2H_2O]$

Complex 2 was synthesized in the same way as complex 1

$[Fe(L)_2(H_2O)_2]$:Color: Reddish-brown, Yield 68.74%, mp, >300 °C, elemental analysis found: C, 63.08; H, 4.68; N, 15.43; Cal, C, 63.16; H, 4.74; N, 15.51; electronic spectra (λ_{max} nm) 440, 510; FT-IR data (KBr, cm^{-1}): 1670 $\nu_{(–CH=N)}$, 1460 $\nu_{(–N=N–)}$; ESI-Mass spectra *m*/*z*: $[C_{38}H_{34}CuN_8O_4+H]^+ = 723.5$.

3.3. DFT Calculations for Ligand, HL

The whole DFT and TD-DFT measurements were recorded on Gaussian 09 software [41], involving the customary exchange-correlation functional B3LYP (Becke, three-parameter, Lee-Yang-Parr) along with basis set 6-31G(d,p) [42,43].On the basis of optimized ground state geometries, electronic transitions and various optimized structural parameters, such as bond lengths, bond angle, and dihedral angles and hormonal vibrational frequency calculation were determined using same

method and basis set. In addition, In addition, few FT-IR vibrations were also shown by animated modes using Gauss View 5 [44]. The parameters such as ΔE, Mulliken electronegativity (χ), dipole moment, chemical potential (μ), global hardness (η), global softness (S), global electrophilicity (ω), absolute softness (σ) and electronic charge (ΔN_{max}) were estimated from the DFT results [45]. The Gauge Independent Atomic Orbital (GIAO) method is used in calculating the NMR spectra in $CDCl_3$ (using the PCM model) and chemical shifts were measured using corresponding TMS shielding at GIAO-B3LYP/6-311G(d,p) level of theory.

3.4. Antimicrobial Assay

The in vitro antimicrobial screening of the ligand and its complexes was studied against the microbes, *Staphylococcus Aureus (Gram positive), Escherichia Coli* (Gram-negative) and *Candida Albicans* and *Aspergillus niger* by Agar well diffusion method [46–49]. A standard inoculums (10^5 CFU/mL) of the microbes was spread on the nutrient agar plates using spreader followed by applying wells of 6 mm diameter filled with 100 μL of tested organisms (1 mg m/L). The agar plates containing microbes were incubated for 24–36 h at 37 °C. The antibiotic chloramphenicol was employed as the standard drug against bacterial strains *Staphylococcus Aureus, Escherichia Coli, while* nystatin was used as antifungal reference drug against *Candida Albicans* and *Aspergillus niger* to be used as positive control at 100 $\mu g/mL^{-1}$ concentration. The susceptibility was determined on the basis of the diameter of the zone of inhibition around the well. All assays were performed at least in duplicate. The dilution test with standard inoculum of 10^5 cfu mL^{-1} was handled to evaluate the minimal inhibitory concentration (MIC) of the ligand test and its complex. Tests with DMSO were used as a negative control, while chloramphenicol and nystatin as a positive control for bacteria and for fungal strains, respectively, and were performed in parallel. The minimal bactericidal concentration (MBC) was determined by aspirating 0.1 mL of culture medium from each tube on agar plates followed by counting of c.f.u. after 18–24 h of incubation at 35 °C. The results of MIC and MBC are given in Table 3.

4. Conclusions

A novel azo-Schiff base ligand and its complexes with Cu(II) ion and Fe(III) ion were reported, and characterized by various physic-chemical methods. All the reported compounds exhibited promising antibacterial activity. However, DFT studies were recorded on ligand and results obtained were comparable with the data existing in literature.

Supplementary Materials: The following are available online, Figure S1: ESI-MS spectrum of ligand, HL.

Acknowledgments: The authors would like to extend their sincere appreciation to the Deanship of Scientific Research at king Saud University for funding this work through research group project number RG -1436-003.

Author Contributions: Mohammad Azam, Saud I. Al-Resayes, and Saikh Mohammad Wabaidur: Design, and collection of data and paper writing, Mohammad Altaf, Nader Talmas M. Albaqami and Mohammad Shahidul Islam: Collection of data, Bhaskar Chaurasia, Satyendra Nath Shukla and Pratiksha Gaur: Synthesis, Mahboob Alam and Soonheum Park: DFT and antimicrobial screening.

Conflicts of Interest: The authors declare no conflict of interest.

References

1. Hunger, K. *Industrial Dyes. Chemistry, Properties, Applications*; Wiley-VCH: Weinheim, Germany, 2003.
2. Sarigul, M.; Kariper, S.E.; Deveci, P.; Atabey, H.; Karakas, D.; Kurtoglu, M. Multi-properties of a new azo-Schiff base and its binuclear copper(II) chelate: Preparation, spectral characterization, electrochemical, potentiometric and modeling studies. *J. Mol. Struct.* **2017**, *1149*, 520–529. [CrossRef]
3. Eren, T.; Kose, M.; Kurtoglu, N.; Ceyhan, G.; McKee, V.; Kurtoglu, M. An azo-azomethine ligand and its copper (II) complex: Synthesis, X-ray crystal structure, spectral, thermal, electrochemical and photoluminescence properties. *Inorg. Chim. Acta* **2015**, *430*, 268–279. [CrossRef]

4. El-Bindary, A.A.; Mohamed, G.G.; El-Sonbati, A.Z.; Diab, M.A.; Hassan, W.M.I.; Morgan, S.M.; Elkholy, A.K. Geometrical structure, potentiometric, molecular docking and thermodynamic studies of azo dye ligand and its metal complexes. *J. Mol. Liq.* **2016**, *218*, 138–149. [CrossRef]
5. Pramanik, A.K.; Sarkar, D.; Mondal, T.K. Electronic structure of thioether containing NSNO donor azo-ligand and its copper(II) complex: Experimental and theoretical studies. *J. Mol. Struct.* **2015**, *1099*, 92–98. [CrossRef]
6. Gup, R.; Giziroglu, E.; Kırkan, B. Synthesis and spectroscopic properties of new azo-dyes and azo-metal complexes derived from barbituric acid and aminoquinoline. *Dyes Pigments* **2007**, *73*, 40–46. [CrossRef]
7. Peters, A.T.; Freeman, H.S. *Colour Chemistry, the Design and Synthesis of Organic Dyes and Pigments*; Elsevier Applied Science: Essex, UK, 1991; p. 193.
8. Gregory, P. *High-Technology Applications of Organic Colorants*; Plenum Press: New York, NY, USA, 1991; p. 1.
9. Catino, S.C.; Farris, R.E. *Concise Encyclopedia of Chemical Technology*; Grayson, M., Ed.; John Wiley & Sons: New York, NY, USA, 1985; p. 142.
10. Ghasemian, M.; Kakanejadifard, A.; Azarbani, F.; Zabardasti, A.; Kakanejadifard, S. Spectroscopy and solvatochromism studies along with antioxidant and antibacterial activities investigation of azo–azomethine compounds 2-(2-hydroxyphenylimino)methyl)-4-phenyldiazenyl)phenol. *Spectrochim. Acta Part A Mol. Biomol. Spectrosc.* **2014**, *124*, 153–158. [CrossRef] [PubMed]
11. Sorochinsky, A.E.; Acena, J.L.; Moriwaki, H.; Sato, T.; Soloshonok, V.A. Asymmetric synthesis of α-amino acids via homologation of Ni(II) complexes of glycine Schiff bases; Part 1: Alkyl halide alkylations. *Amino Acids* **2013**, *45*, 691–718. [CrossRef] [PubMed]
12. Sorochinsky, A.E.; Acena, J.L.; Moriwaki, H.; Sato, T.; Soloshonok, V.A. Asymmetric synthesis of α-amino acids via homologation of Ni(II) complexes of glycine Schiff bases. Part 2: Aldol, Mannich addition reactions, deracemization and (S) to (R) interconversion of α-amino acids. *Amino Acids* **2013**, *45*, 1017–1033. [CrossRef] [PubMed]
13. Acena, J.L.; Sorochinsky, A.E.; Soloshonok, V. Asymmetric synthesis of alpha-amino acids via homologation of Ni(II) complexes of glycine schiff bases. Part 3: Michael addition reactions and miscellaneous transformations. *Amino Acids* **2014**, *46*, 2047–2073. [CrossRef] [PubMed]
14. Acena, J.L.; Sorochinsky, A.E.; Moriwaki, H.; Sato, T.; Soloshonok, V.A. ChemInform Abstract: Synthesis of Fluorine-Containing α-Amino Acids in Enantiomerically Pure Form via Homologation of Ni(II) Complexes of Glycine and Alanine Schiff Bases. *J. Fluor. Chem.* **2013**, *155*, 21–38. [CrossRef]
15. Al-Resayes, S.I.; Shakir, M.; Shahid, N.; Azam, M.; Khan, A.U. Synthesis, spectroscopic characterization and in vitro antimicrobial studies of Schiff base ligand, H2L derived from glyoxalic acid and 1,8-diaminonaphthalene and its Co(II), Ni(II), Cu(II) and Zn(II) complexes. *Arab. J. Chem.* **2016**, *9*, 335–343. [CrossRef]
16. Santosa, A.F.; Brottoa, D.F.; Favarina, L.R.V.; Cabezaa, N.A.; Andrade, G.R.; Batistote, M.; Alberto, A.; AdemirNeves, C.; Rodrigues, D.C.M.; dos Anjos, A. Study of the antimicrobial activity of metal complexes and their ligands through bioassays applied to plant extracts. *Rev. Bras. Farmacogn.* **2014**, *24*, 309–315. [CrossRef]
17. Lewandowski, E.M.; Lethbridge, K.G.; Sanishvili, R.; Skiba, J.; Kowalski, K.; Chen, Y. Mechanisms of proton relay and product release by Class A β-lactamase at ultrahigh resolution. *FEBS J.* **2018**, *285*, 87–100. [CrossRef] [PubMed]
18. Lewandowski, E.M.; Szczupak, L.; Wong, S.; Skiba, J.; Guśpiel, A.; Solecka, J.; Vrček, V.; Kowalski, K.; Chen, Y. Antibacterial Properties of Metallocenyl-7-ADCA Derivatives and Structure in Complex with CTX-M β-Lactamase. *Organometallics* **2017**, *36*, 1673–1676. [CrossRef] [PubMed]
19. Wenzel, M.; Patra, M.; Senges, C.H.R.; Ott, I.; Stepanek, J.J.; Pinto, A.; Prochnow, P.; Vuong, C.; Langklotz, S.; Metzler-Nolte, N.; et al. Analysis of the Mechanism of Action of Potent Antibacterial Hetero-tri-organometallic Compounds: A Structurally New Class of Antibiotics. *ACS Chem. Biol.* **2013**, *8*, 1442–1450. [CrossRef] [PubMed]
20. Patra, M.; Gasser, G.; Metzler-Nolte, N. Small organometallic compounds as antibacterial agents. *Dalton Trans.* **2012**, *41*, 6350–6358. [CrossRef] [PubMed]
21. Albada, H.B.; Prochnow, P.; Bobersky, S.; Bandow, J.E.; Metzler-Nolte, N. Highly active antibacterial ferrocenoylated or ruthenocenoylated Arg-Trp peptides can be discovered by an L-to-D substitution scan. *Chem. Sci.* **2014**, *5*, 4453–4459. [CrossRef]

22. Jabłonski, A.; Matczak, K.; Koceva-Chyła, A.; Durka, K.; Steverding, D.; Jakubiec-Krzesniak, K.; Solecka, J.; Trzybinski, D.; Wozniak, K.; Andreu, V.; et al. Cymantrenyl-Nucleobases: Synthesis, Anticancer, Antitrypanosomal and Antimicrobial Activity Studies. *Molecules* **2017**, *22*, 2220. [CrossRef] [PubMed]
23. Khanmohammadi, H.; Darvishpour, M. New azo ligands containing azomethine groups in the pyridazine-based chain: Synthesis and characterization. *Dyes Pigments* **2009**, *81*, 167–173. [CrossRef]
24. El-Baradie, K.; El-Sharkawy, R.; El-Ghamry, H.; Sakai, K. Synthesis and characterization of Cu(II), Co(II) and Ni(II) complexes of a number of sulfadrug azodyes and their application for wastewater treatment. *Spectrochim. Acta Part A* **2014**, *121*, 180–187. [CrossRef] [PubMed]
25. Shakir, M.; Azam, M.; Ullah, M.F.; Hadi, S.M. Synthesis, spectroscopic and electrochemical studies of N,N-bis[(E)-2-thienylmethylidene]-1,8-naphthalenediamine and its Cu(II) complex: DNA cleavage and generation of superoxide anion. *J. Photochem. Photobiol. B* **2011**, *104*, 449–456. [CrossRef] [PubMed]
26. Warad, I.; Khan, A.A.; Azam, M.; Al-Resayes, S.I.; Haddad, S.F. Design and structural studies of diimine/CdX_2 (X = Cl, I) complexes based on 2,2-dimethyl-1,3-diaminopropane ligand. *J. Mol. Struct.* **2014**, *1062*, 167–173. [CrossRef]
27. Azam, M.; Al-Resayes, S.I.; Velmurugan, G.; Venuvanalingam, P.; Wagler, J.; Kroke, E. Novel uranyl(vi) complexes incorporating propylene-bridged salen-type N_2O_2-ligands: A structural and computational approach. *Dalton Trans.* **2015**, *44*, 568–577. [CrossRef] [PubMed]
28. Sheikhshoaie, I.; Saheb, V. A new salen base 5-(phenylazo)-N-(2-amino pyridine) salicyliden Schiff base ligand: Synthesis, experimental and density functional studies on its crystal structure, FTIR, ^{1}H-NMR and 13C NMR spectra. *Spectrochim. Acta Part A* **2010**, *77*, 1069–1076. [CrossRef] [PubMed]
29. Wu, S.; Qian, W.; Xia, Z.; Zou, Y.; Wan, S.; Shen, S. Investigation of third-order nonlinearity of an azo dye and its metal-substituted compounds. *Chem. Phys. Lett.* **2000**, *330*, 535–540. [CrossRef]
30. Manonmani, J.; Kandaswamy, M.; Narayanan, V.; Thirumurugan, R.; Sundura, S.S.; Shanmugam, G.; Ponnuswamy, M.N.; Fun, H.K. Synthesis of copper(II) and nickel(II) complexes using compartmental ligands: X-ray, electrochemical and magnetic studies. *Polyhedron* **2001**, *20*, 3039. [CrossRef]
31. Cotton, F.A.; Wilkinson, G. *Advanced Inorganic Chemistry*, 5th ed.; Wiley: New York, NY, USA, 1988.
32. Firdaus, F.; Fatma, K.; Azam, M.; Khan, S.N.; Khan, A.U.; Shakir, M. Template synthesis and physicochemical studies of 14-membered hexaazmacrocyclic complexes with Co(II), Ni(II), Cu(II) and Zn(II): A comparative spectroscopic approach on DNA binding with Cu(II) and Ni(II) complexes. *Trans. Met. Chem.* **2008**, *33*, 467–473. [CrossRef]
33. Masoud, M.S.; El-Dussouky, A.; Ghatwary, E.E. Geometry of New Iron (III) and Copper (II) Azo-Nitroso complexes Trans. *Met. Chem.* **1986**, *11*, 161–164. [CrossRef]
34. Fukui, K.; Yonezawa, T.; Shingu, H.J. A Molecular Orbital Theory of Reactivity in Aromatic Hydrocarbons. *J. Chem. Phys.* **1952**, *20*, 722–725. [CrossRef]
35. Lynam, M.M.; Kuty, M.; Damborsky, J.; Koca, J.; Adriaens, P. Molecular orbital calculations to describe microbial reductive dechlorination of polychlorinated dioxins. *Environ. Toxicol. Chem.* **1998**, *17*, 988–997. [CrossRef]
36. Alam, M.; Alam, M.J.; Azaz, S.; Parveen, M.; Park, S.; Ahmad, S. DFT/TD-DFT calculations, spectroscopic characterizations (FTIR, NMR, UV-vis), molecular docking and enzyme inhibition study of 7-benzoyloxycoumarin. *Comput. Biol. Chem.* **2018**, *73*, 65–78. [CrossRef] [PubMed]
37. Orojloo, M.; Zolgharnein, P.; Solimannejad, M.; Amani, S. Synthesis and characterization of cobalt (II), nickel (II), copper (II) and zinc (II) complexes derived from two Schiff base ligands: Spectroscopic, thermal, magnetic moment, electrochemical and antimicrobial studies. *Inorg. Chim. Acta* **2017**, *467*, 227–237. [CrossRef]
38. Patel, R.N.; Singh, Y.; Singh, Y.P.; Butcher, R.J.; Kamal, A.; Tripathi, I.P. Copper(II) and nickel(II) complexes with N′-[(Z)-phenyl(pyridin-2-yl)methylidene]acetohydrazide: Synthesis, crystal structures, DFT calculations and antioxidant effects. *Polyhedron* **2016**, *117*, 20–34. [CrossRef]
39. Bandyopadhyay, A.; Higuchi, M. From metal complexes to metallosupramolecular polymers via polycondensation: Synthesis, structure and electrochromic properties of Co(III)- and Fe(III)-based metallosupramolecular polymers with aromatic azo ligands. *Eur. Polym. J.* **2013**, *49*, 1688–1697. [CrossRef]
40. Ferro, R.; Milione, S.; Caruso, T.; Grassi, A. Iron(III) complexes of bidentate nitrogen ligands as catalysts in reverse atom transfer radical polymerization of styrene. *J. Mol. Catal. A Chem.* **2009**, *307*, 128–133. [CrossRef]
41. Frisch, M.J. *Gaussian 09, Revision D.01*; Gaussian Inc.: Wallingford, CT, USA, 2009.

42. Beck, A.D. Density-functional exchange-energy approximation with correct asymptotic behaviour. *Phys. Rev. A* **1988**, *38*, 3098–3100. [CrossRef]
43. Lee, C.; Yang, W.; Parr, R.G. Development of the colle-salvetticorrelationenergy formula into a functional of the electron density. *Phys. Rev. A* **1988**, *37*, 785–789.
44. Dennington, R.; Keith, T.; Millam, J. *GaussView*; Ver. 5; Semichem Inc.: Shawnee Mission, KS, USA, 2009.
45. Chermette, H. Chemical reactivity indexes in density functional theory. *J. Comput. Chem.* **1999**, *20*, 129–154. [CrossRef]
46. Perez, C.; Pauli, M.; Bazerque, P. An antibiotic assay by the agar well diffusion method. *Acta Biol. Med. Exp.* **1990**, *15*, 113–115.
47. Aqil, F.; Khan, M.S.A.; Ahmed, I. Effect of certain bioactive plant extracts on clinical isolates of beta-lactamase producing methicillin resistant Staphylococcus aureus. *J. Basic Microbiol.* **2005**, *45*, 106–114. [CrossRef] [PubMed]
48. Cruickshank, R.; Duguid, J.P.; Marmion, B.P.; Swain, R.H.A. *Medicinal Microbiology*, 12th ed.; Churchill Livingstone: London, UK, 1975; Volume 2, pp. 196–202.
49. Doughari, J.H.; Nuya, S.P. In Vitro antifungal activity of deterium microcarpum. *Pak. J. Med. Sci.* **2008**, *24*, 91–95.

Sample Availability: Samples of the compounds are available from the authors.